KSME

Springer

Journal of Mechanical Science and Technology 36 (11) 2022

Original Article
DOI 10.1007/s12206-022-1003-z

Keywords:
· Active vibration control system (AVCS)
· Airframe vibration reduction
· UH-60A helicopter
· Human body vibration

Correspondence to:
Jae-Sang Park
aerotor@cnu.ac.kr

Citation:
Park, B.-H., Bang, S.-W., Lee, Y.-L., Park, J.-S. (2022). Active vibration reductions for airframe and human body of UH-60A helicopter in low- and high-speed flights. Journal of Mechanical Science and Technology 36 (11) (2022) 5363~5373. http://doi.org/10.1007/s12206-022-1003-z

Received April 13th, 2022
Revised July 7th, 2022
Accepted July 14th, 2022

† Recommended by Editor
No-cheol Park

Active vibration reductions for airframe and human body of UH-60A helicopter in low- and high-speed flights

Byeong-Hyeon Park[1], Shin-Won Bang[1], Ye-Lin Lee[2] and Jae-Sang Park[1]

[1]Department Aerospace Engineering, Chungnam National University, Daejeon 34134, Korea, [2]Spacecraft Structure Team, Satrec Initiative, Daejeon 34054, Korea

Abstract A simulation study using an active vibration control system (AVCS) is conducted to reduce the vibration responses of UH-60A helicopter airframe and human body on a pilot seat in both low-and high-speed flights (μ = 0.15 and μ = 0.37). The 4P hub vibratory loads of the UH-60A helicopter are calculated using DYMORE II, a nonlinear multibody dynamics analysis code, and MSC. NASTRAN is used to predict the vibration responses of the UH-60A airframe and human body. MATLAB Simulink is used to construct the AVCS framework using seven accelerometers and five force generators. The AVCS in this study uses Fx-LMS algorithm to determine vibration-cancellation forces. When applying the AVCS to the UH-60A helicopter, the 4P airframe vibration response reductions at low-and high-speed flight conditions are 22.05 % to 97.83 % and 25.05 % to 91.81 %, respectively. The vibration responses of the human body are reduced from 89.29 % to 90.16 % and 61.23 % to 72.43 % at low-and high-speed flight conditions, respectively.

1. Introduction

A helicopter has various rotating parts, such as rotor systems, transmissions, and engines, which cause vibration of the airframe. Among the various helicopter vibration sources, the main rotor vibration has a dominant effect and it is transferred to the airframe through the rotor hub. In addition, owing to the unique dynamic characteristics of the rotor system, the rotor excites the airframe with the harmonic frequency (nN_b/rev), which is the number of blades per rotor (N_b) multiplied by the integer number (n), where 1/rev (1P) is the non-dimensionalized rotating speed of the rotor. The vibration transferred from the rotor hub significantly affects the fatigue life of the structure, electronic equipment, and passenger comfort; therefore, it is important to reduce airframe vibration.

Passive and active vibration control techniques have been applied to reduce helicopter vibration. The passive vibration reduction technique uses a vibration absorber at the rotor head mount, which is the path of vibration transmitted from the rotor, or mounting the vibration absorber in a part that requires vibration reduction of the airframe. However, passive vibration reduction techniques have the disadvantage of increasing the drag and weight, and it is possible to achieve good vibration reduction performance only in narrow frequency bands. On the other hand, the active vibration reduction technique is a method of reducing airframe vibration by generating a controllable force opposite to the airframe vibration, and it has better vibration reduction performance at a wider frequency than the passive vibration reduction technique.

Among various active vibration control techniques, the active vibration control system (AVCS) uses accelerometers and force generators [1], and a closed-loop feedback control algorithm generates vibration cancellation signals that have the same magnitude and opposite phase to the airframe vibration signals. The AVCS has a better vibration reduction performance in wider frequency bands compared to conventional passive vibration control techniques.

AVCS has been applied to lift-offset coaxial compound helicopters, such as X2 technology

demonstrators (Fig. 1(a), [2]), S-97 Raider (Fig. 1(b)), and SB>1 Defiant (Fig. 1(c)), and conventional helicopters, such as UH-60M (Fig. 1(d), [3] and S-92 (Fig. 1(e), [4]). In addition, the V-22 tiltrotor aircraft uses an AVCS (Fig. 1(f), [5]). These applications of AVCS to various rotorcraft demonstrate an excellent reduction in airframe vibrations.

Two flight speed conditions generate extreme vibrations in helicopters: a low-speed flight condition (approximately advance ratio, μ = 0.15) with blade vortex interaction (BVI) and a high-speed flight condition (approximately μ = 0.37) accompanied by compressibility effects on the advancing side of the rotor. To reduce the vibrations using AVCS successfully, the optimization of the number of force generators and their locations is required because the vibration reduction performance depends on the number and locations of force generators. However, the number and locations of the force generators optimized to effectively reduce the airframe vibration at a given flight condition may not guarantee good vibration reduction performance at another flight condition. Thus, it is important to simultaneously optimize the number and locations of force generators at both low-and high-speed flight conditions. Although the number of force generators for the UH-60A helicopter was determined and the force generators were placed optimally for the high-speed flight condition of the helicopter by the present authors [6], research to determine optimally the locations of force generators has not been conducted to control the airframe vibration in low-speed flight. Furthermore, optimization studies have not been conducted to design the locations of force generators to reduce airframe vibration appropriately at both low- and high-speed flight conditions.

Pilots and passengers are exposed to human body vibrations by helicopter airframe vibrations, which may cause several problems in the human body. It has been reported that the human body vibration significantly affects the working conditions of pilots, and many helicopter pilots experience neck and low back pain during flights [7, 8]. In addition, helicopter pilots are much more likely to have musculoskeletal disorders in low- and high-speed flights with severe vibrations. Thus, it is necessary to alleviate the human body vibrations by reducing helicopter airframe vibrations.

This study aims to control helicopter airframe vibrations at both low- and high-speed flight conditions, using AVCS simulation. A UH-60A helicopter is considered for this study, and the authors' previous work results [6] for the AVCS simulation of a UH-60A helicopter at high-speed flight condition (158 knots) are used as the baseline. Therefore, the MSC.NASTRAN model of the UH-60A airframe with a one-dimensional (1D) stick (elastic line) model and the AVCS simulation framework based on MATLAB Simulink are obtained from Ref. [6]. The 4/rev hub vibratory loads of the UH-60A rotor at low-speed flight condition (64 knots) are obtained from a previous analysis [9] using DYMORE II, a nonlinear flexible multibody dynamics analysis code [10]. In this study, the force generator locations for the AVCS simulation are optimally determined to reduce UH-60A airframe vibrations at both low- and high-speed flight conditions. In addition, the reductions in pilot's body vibration are investigated when AVCS is applied to the UH-60A helicopter.

(a) X2TD (b) S-97 Raider

(c) SB>1 Defiant (d) UH-60M

(e) S-92 (f) V-22

Fig. 1. Various helicopters using AVCS.

2. Simulation methods

2.1 UH-60A helicopter and flight conditions

In this study, the UH-60A helicopter (Fig. 2 and Table 1) is used because various and extensive measured or predicted data are available for performance, loads, vibration, acoustic noise in the public domain [11, 12]. Table 2 summarizes the two flight conditions for the UH-60A helicopter. At the high-speed flight condition (flight counter 8534), the compressibility effect on the rotor advancing side causes serious vibration [13], whereas the BVI produces vibration at the low-speed flight condition (flight counter 8513, [9]).

Table 1. General properties of UH-60A helicopter.

Gross weight		16850 lb
Main rotor	Number of blades, N_b	4
	Radius, R	26.83 ft
	Nominal chord, c	1.73 ft
	Pretwist	-16.0 deg. (nonlinear)
	Solidity, σ	0.0826
	Nominal rotor speed	258 RPM
	Airfoils	SC 1095/SC1094R8
Fuselage	Length	50.09 ft
	Height	16.83 ft
	Width	7.74 ft

Table 2. Flight conditions of UH-60A helicopter.

Flight counter	8513 [9]	8534 [13]
Advance ratio, μ	0.150 (64 knots)	0.368 (158 knots)
Thrust coefficient, C_T/σ	0.076	0.084
Tip mach No.	0.644	0.642
Altitude	3080 ft	3273 ft
Shaft tilting angle, α_s	0.75 deg.	-7.31 deg.

Fig. 2. UH-60A helicopter.

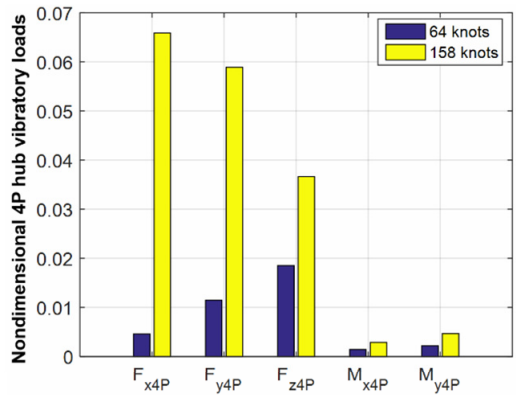

Fig. 3. Nondimensional 4P vibratory hub loads of UH-60A.

2.2 Rotor-airframe coupling method

A one-way coupling method is used to predict the vibration responses of the UH-60A helicopter airframe. In this approach, the rotor and airframe are modeled separately using DYMORE II [10], a flexible multibody dynamics analysis code, and MSC.NASTRAN, a commercial finite element analysis program. First, the isolated UH-60A rotor is trimmed to satisfy the flight conditions listed in Table 2, and 4P hub vibratory loads are obtained [9, 13] (Fig. 3). Second, the 4P hub vibratory loads predicted by DYMORE II excites the UH-60A airframe structure modeled using MSC.NASTRAN, and 4P airframe vibration responses are calculated using MSC.NASTRAN. In the one-way coupling approach, based on a previous study [14], the motion of the airframe is not considered in the rotor analysis, unlike the two-way coupling approach, which is a fully coupled analysis. The one-way coupling technique is simpler than the two-way coupling method; however, it can also appropriately predict the vibration responses of an airframe excited by the hub vibratory loads of a rotor [14]. The 4P hub vibratory loads of a UH-60A rotor at low- and high-speed flight conditions are obtained from the authors' previous studies [9, 13] using DYMORE II. The nondimensional 4P hub vibratory loads [9, 13] are presented in Fig. 3. Detailed descriptions can be found in Refs. [9, 13].

2.3 Structural dynamic modeling of the airframe

Compared with the three-dimensional (3D) model, the 1D model is simpler and consist of a smaller number of elements; however, the 1D model can also appropriately present dynamic characteristics. Using MSC.NASTRAN, two different 1D stick models are modeled in this work to represent the airframe structure of the UH-60A helicopter: a normal mode analysis model and a ground vibration test (GVT) model. The normal mode analysis model consists of 41 elastic beam elements (CBAR) and 26 lumped mass elements, and it calculates the natural frequencies of the airframe structure under free-free boundary conditions. Based on the normal mode analysis model, the GVT model is constructed to predict the 4P vibration responses during flights. The GVT model is constructed by adding the bungee cables to the normal mode analysis model. When the material properties and lengths of cables are adjusted appropriately, the GVT model can be designed so that the GVT model's natural frequencies are quite similar to those of the normal mode analysis model in free-free boundary conditions; therefore, the GVT model can represent the helicopter airframe dynamic characteristics in flights. When the GVT model is used to predict the airframe vibration responses in flights, the full aircraft trim is not required, and the analysis is quite simple based on the one-way coupling approach. Therefore, the normal mode analysis model is a reference dynamics model for the GVT model, which is used to calculate the UH-60A airframe vibration responses. Because further detailed modeling techniques of 1D stick airframe structures are presented in previous research [6], this study summarizes the analysis results of previous works. Fig. 4 shows the normal mode analysis mode (Fig. 4(a)) and GVT model (Fig. 4(b)) of the UH-60A helicopter using a 1D stick airframe model. The natural frequencies of the normal mode analysis model, shake test of the UH-60A helicopter [15], and natural frequencies obtained by frequency response analysis for the GVT model are presented in Table 3.

2.4 Structural dynamics modeling of a human body

To predict the pilot's body vibration, the structural dynamics modeling of the human body is modeled using the finite element structural analysis program, MSC.NASTRAN (Fig. 5). A human body model is constructed using 1D beam elements (CBAR) and concentrated mass elements. The node locations, mass properties, and stiffness data for the human body model are obtained from Ref. [16]. The model is based on a human

Table 3. Natural frequencies of the UH-60A airframe model.

Fuselage bending mode	Natural frequencies [Hz]			
	Shake test [15]	Prediction [15]	Present	
			Normal mode analysis model	GVT model
1st lateral mode	5.58	5.40	5.40	5.40
1st vertical mode	6.79	6.49	6.49	6.60
2nd vertical mode	14.01	14.52	14.52	14.40
2nd lateral mode	N/A	16.57	16.57	16.50

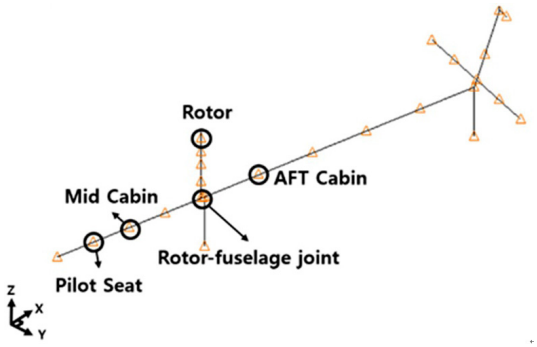

(a) Normal mode analysis model in free-free boundary conditions

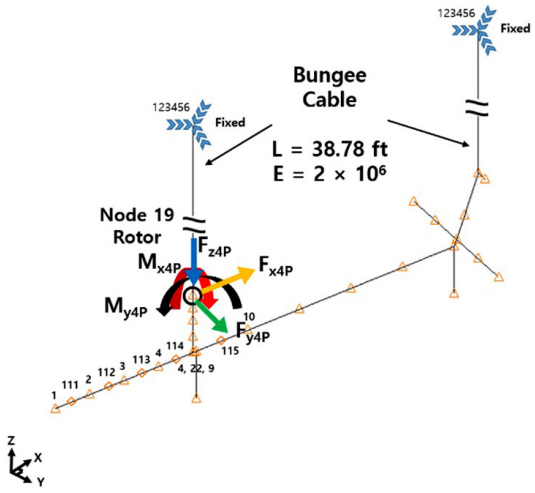

(b) Ground vibration test (GVT) model

Fig. 4. 1D stick models of the UH-60A helicopter.

upper body with a body mass of approximately 60 kg. The human body model includes different major parts such as the spine, ribs, head, pelvis, and viscera. Furthermore, these major parts are simplified as lumped masses at the locations of their centers of gravity. The masses in the upper arms are included in the torso masses. To account for the dynamic characteristics of the thighs and hands, a portion of their weights is added to the pelvic mass. The material properties are assumed to appropriately represent the natural frequencies of a human body, as given in Ref. [16].

Table 4. Natural frequencies of human body model.

Bending mode no.	Natural frequencies [Hz]		Difference [%]
	Ref. [16]	Present	
1	0.28	0.39	38.57
2	1.49	1.04	-29.74
3	2.81	2.81	0.10
4	5.06	4.71	-6.92
5	5.77	5.27	-8.69

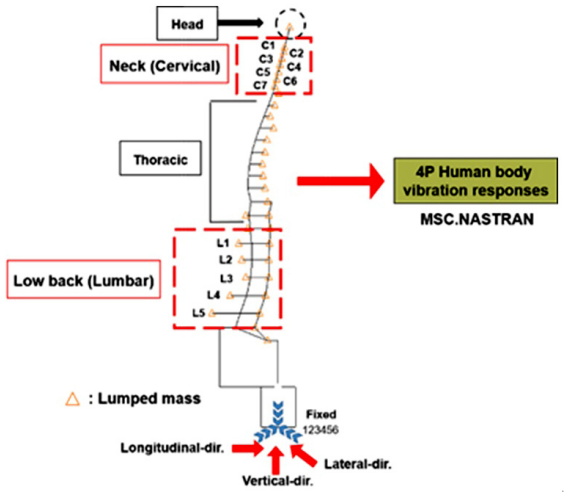

Fig. 5. Structural dynamic model of a human body.

A normal mode analysis is conducted to predict the natural frequencies of the human body model sitting on a pilot seat. The natural frequencies of the five lower-bending modes are listed in Table 4. When comparing the present results with those in Ref. [16], the error is not small; however, the present model can reasonably represent the structural dynamics of the human body on the pilot seat.

For the vibration of a seated human body exposed to helicopter vibration, the vertical motions have the most significant effect on the human body [17]. In addition, as previously discussed in Introduction, neck and low back pain due to vibrations adversely affects the working conditions and comfort of helicopter pilots during flights [7, 8]. Therefore, this study using AVCS aims to alleviate the 4P human body vibration responses in the vertical direction at the cervical and lumbar regions of the human body. First, the 4P airframe vibrations of the UH-60A helicopter with or without an AVCS at both flight conditions excite the bottom of the human body model. Second, the vibration responses of the human body at specified locations are investigated.

2.5 AVCS

As shown in Fig. 6, the AVCS alleviates airframe vibrations using accelerometers, force generators [18], and a closed-loop

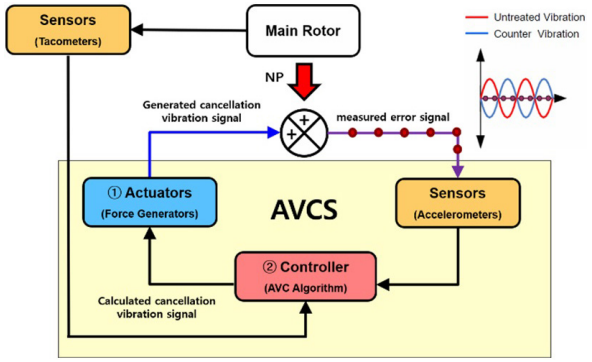

Fig. 6. Block diagrams of active vibration control system [6].

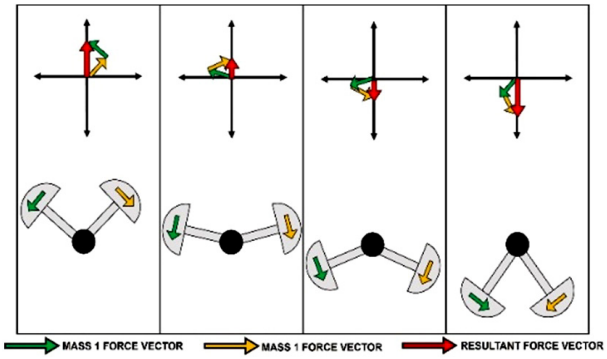

Fig. 7. Force vector of counter rotating force generator [1].

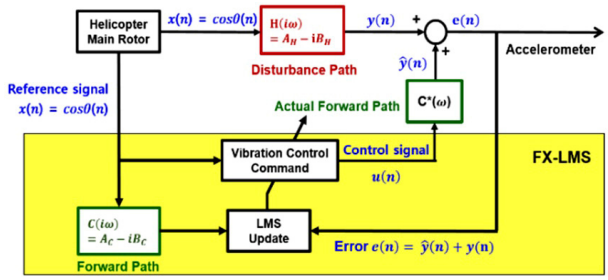

Fig. 8. Block diagrams of Fx-LMS algorithm [6].

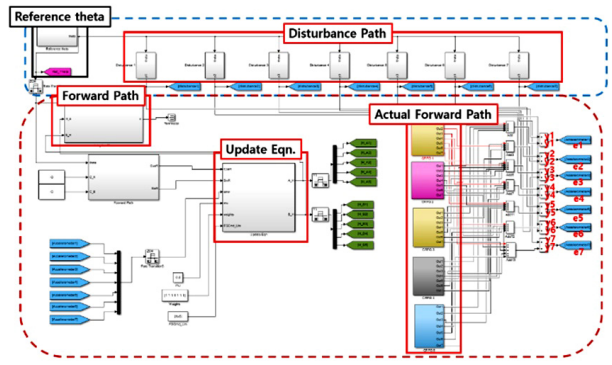

Fig. 9. Block diagrams of AVCS framework.

feedback controller. First, accelerometers measure the vibration response signals of the helicopter airframe, and the controller predicts the vibration cancellation signals that have the same magnitude but are in the opposite direction to the airframe vibration response signals. Finally, using the determined vibration cancellation signals, the force generators produce vibration cancellation forces that can reduce the airframe vibration responses.

In this study, counter-rotating force generators (CRFGs) are considered. The CRFG uses two disks that have imbalanced rotating masses with relative angles, and it produces a linear centrifugal force (Fig. 7). Detailed information on the CRFG used in this study can be obtained from the previous work of the authors [6].

The controller uses the Filtered-x least mean square (Fx-LMS) algorithm that has been extensively applied for active noise and vibration reduction. As shown in Fig. 8, the Fx-LMS algorithm uses three types of signals: the airframe vibration response signals (y(n)), vibration cancellation signals generated from CRFGs (ŷ(n)), and error signals (e(n)), which are the sum of the vibration response signals and the vibration cancellation signals. To minimize the error signal (e(n)), the Fx-LMS algorithm uses the gradient descent method. Further detailed descriptions of AVCS are provided in Refs. [1, 6].

The AVCS in this study uses a multi-input multi-output (MIMO) system with seven accelerometers and five CRFGs [6]. AVCS reduces airframe vibration responses at the specified locations and in the given directions since the limited number of CRFGs are used considering weight increase. Thus, the specified airframe locations should be carefully selected where the vibration responses needed to be alleviated. Accelerometers are located where vibration reductions are required, such as a pilot seat, mid-cabin, rotor-fuselage joint, and after-cabin based on the previous works [3, 6]. Because the vibration reduction performance depends on both the locations and vibration cancellation force directions of the CRFGs, ten simulation studies are conducted to alleviate effectively the airframe vibration responses at both low- and high-speed flight conditions for the UH-60A helicopter.

The AVCS framework [6] using the Fx-LMS algorithm is modeled using MATLAB Simulink (Fig. 9). The reference theta is the 4P phase angle, which is used for the input values of the disturbance path and Fx-LMS algorithm. The disturbance path represents the dynamic characteristics of the UH-60A helicopter airframe structure, and the output value of the disturbance path (y(n)) shows the 4P vibration-response signals of the airframe model. The control algorithm includes the forward path, which represents the dynamic characteristics of the actuators, and an actual forward path, which is a mathematical transfer function of the actuators. Furthermore, to determine the vibration cancellation signals, the system identification coefficients of the mathematical transfer function of the forward path must be calculated. In the system identification, the entire system is assumed to be linear time invariant, and the LMS update equation is applied to calculate the system identification coefficients [18].

3. Numerical results

3.1 Airframe vibration reduction using AVCS

3.1.1 Vibration reduction at high-speed flight condition

In Ref. [6], the locations and force directions of CRFGs were determined for the best vibration reduction of the UH-60A helicopter airframe at a high-speed flight condition (μ = 0.37). Therefore, this study summarizes the results given in Ref. [6], as shown in Figs. 10 and 11. Fig. 10 shows the locations and force directions of the five force generators. When the AVCS system in Fig. 10 is applied to the UH-60A helicopter at μ = 0.37, the airframe vibration reductions are plotted in Fig. 11 [6]. The vertical vibration responses at the pilot seat, mid-cabin, and rotor-fuselage joint are reduced by 52.02-82.17 %, and the vibration reductions in the longitudinal direction are 28.35-90.17 %. In addition, the lateral vibration response at the aft-cabin is reduced by 92.94 %.

3.1.2 Vibration reduction at low-speed flight condition

A case study is conducted to determine the locations and force directions of the CRFGs at the low-speed flight condition (μ = 0.15). Table 5 summarizes the arrangements of the five CRFGs for AVCS, and case 1 represents the CRFG arrangement in Fig. 10, which is the best case at 158 knots. The airframe vibration control performance is evaluated using Eq. (1).

$$J = \sum_{i=1}^{7} (r_i w_i) \tag{1}$$

where J is the cost function, r_i is the percentage change (%) of the i^{th} accelerometer, and w_i is the weighting factor. The largest weighting factor is assigned to the 2^{nd} accelerometer (the longitudinal direction accelerometer at the pilot seat) because this airframe vibration response is the most difficult to alleviate. Furthermore, the smallest weighting factor is assigned to the 7^{th} accelerometer (lateral direction accelerometer at the aft-cabin). Table 6 summarizes the airframe vibration reductions using AVCS. As presented in the table, although case 1 is the best case at 158 knots in the previous work [6], the airframe vibration reduction using case 1 at 64 knots is not the best; therefore, it is determined that the best arrangement of CRFGs at a low-speed flight condition is different from that at a high-speed flight condition. However, case 6 shown in Fig. 12 shows the largest value of J; thus, it is considered the best case for alleviating the UH-60A airframe vibration responses at low-speed flight condition. Fig. 13 shows the airframe vibration

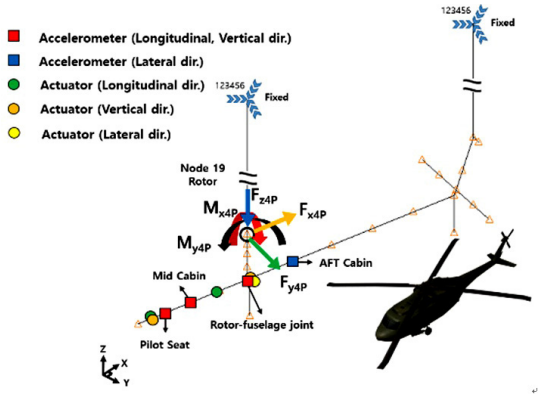

Fig. 10. Best case for high-speed flight condition [6].

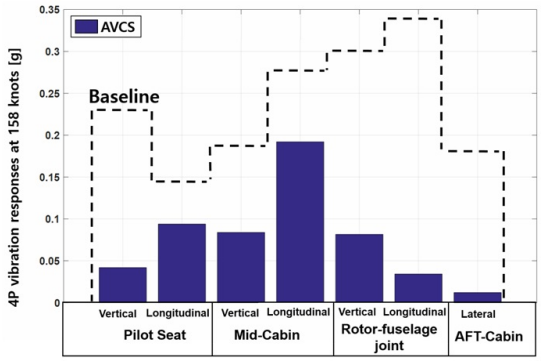

Fig. 11. 4P vibration reduction using AVCS at high-speed flight condition [6].

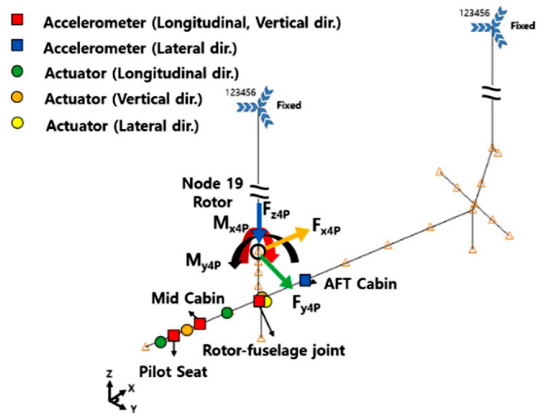

Fig. 12. Vibration response analysis model using AVCS (case 6).

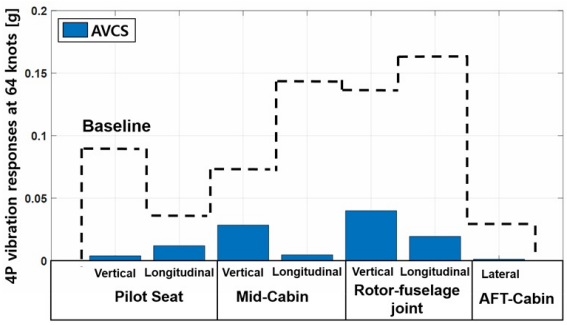

Fig. 13. 4P vibration reduction using AVCS at low-speed flight condition (case 6).

Table 5. Locations of CRFGs for the case study at the low-speed flight condition.

Case	Longitudinal direction	Vertical direction	Lateral direction
1	Node 111, 22	Node 111, 9	Node 9
2	Node 112, 19	Node 112, 19	Node 10
3	Node 112, 19	Node 112, 19	Node 9
4	Node 112, 19	Node 112, 19	Node 9
5	Node 111, 9	Node 111, 9	Node 9
6	Node 111, 19	Node 112, 9	Node 9

Table 6. Reductions of 4P vibration responses of UH-60A airframe using AVCS at low-speed flight condition.

	Vibration reduction using AVCS [%]							
Case	ACC1	ACC2	ACC3	ACC4	ACC5	ACC6	ACC7	J
1	88.7	25.1	61.0	81.9	62.9	81.8	91.96	68.4
2	47.9	-35.7	71.8	95.7	98.1	7.7	69.7	47.6
3	49.9	-41.0	74.6	94.5	98.1	7.7	86.2	48.9
4	73.7	44.4	78.8	97.4	-2.4	9.0	95.1	54.8
5	35.8	-43.1	-52.1	29.1	97.8	97.5	84.8	31.0
6	**95.3**	**67.3**	**55.5**	**96.5**	**68.6**	**87.0**	**95.5**	**79.8**
w_i	0.14	0.17	0.15	0.15	0.14	0.15	0.1	

Table 7. Locations of CRFGs for the case study for the low- and high-speed flight conditions.

Case	Longitudinal direction	Vertical direction	Lateral direction
1	Node 112, 19	Node 112, 19	Node 10
2	Node 112, 19	Node 112, 19	Node 9
3	Node 112, 19	Node 112, 19	Node 9
4	Node 111, 9	Node 111, 9	Node 9
5	Node 111, 19	Node 112, 9	Node 9
6	Node 2, 9	Node 2, 9	Node 9
7	Node 112, 9	Node 112, 9	Node 9
8	Node 1, 9	Node 1, 9	Node 9
9	Node 3, 9	Node 1, 9	Node 9
10	Node 112, 9	Node 1, 9	Node 9

reductions when the AVCS with case 6 is applied to the UH-60A helicopter at μ = 0.15. As shown in the figure, the 4P vibration responses at the seven accelerometers are reduced by 55.49 %-96.45 % compared to the baseline response without AVCS. At the pilot seat, the 4P vertical vibration response is reduced by 95.31 %, and the 4P vibration response in the longitudinal direction is alleviated by 67.3 % compared to the baseline response without AVCS. The 4P vibration response in the vertical direction is reduced by 55.49 %, and the reduction in the 4P longitudinal vibration response is 96.45 % at the mid-cabin. At the rotor-fuselage joint, the 4P vibration responses in the vertical and longitudinal directions are reduced by 68.62 % and 86.99 %, respectively, from the baseline without the AVCS. The 4P vibration response in the lateral direction the after-cabin is reduced by 95.54 %, compared to baseline response. All the airframe vibrations reduced are less than 0.1 g when the AVCS with case 6 is used for the UH-60A helicopter.

3.1.3 Vibration reduction at low- and high-speed flight conditions

Based on the results presented in the previous sections, a case study is conducted to determine the locations and force directions of CRFGs to alleviate effectively the UH-60A airframe vibration responses at both low- and high-speed flight conditions (μ = 0.15 and 0.34). Table 7 summarizes the locations and force directions of the CRFGs for the ten cases used in this section. Fig. 14 shows the reductions in 4P airframe vibration responses at both flight conditions when ten cases are considered. Compared to the baseline result without AVCS, the vibration responses decrease considerably. Similar to Sec. 3.1.2, the vibration reduction performances of ten cases are evaluated using Eq. (2).

Table 8. Reductions of 4P vibration responses of UH-60A airframe using AVCS at low- and high-speed flight conditions.

Vibration reduction [%]															
Low-speed flight condition (μ = 0.15)								High-speed flight condition (μ = 0.37)							
Case	Acc1	Acc2	Acc3	Acc4	Acc5	Acc6	Acc7	Acc1	Acc2	Acc3	Acc4	Acc5	Acc6	Acc7	J
1	47.9	-35.7	71.8	95.7	98.1	7.7	69.7	11.5	2.2	26.3	82.3	67.9	2.6	90.0	38.8
2	49.9	-41.0	74.6	94.5	98.1	7.7	86.2	15.3	-1.6	29.8	82.0	68.5	1.0	95.8	39.5
3	73.7	44.4	78.8	97.4	-2.4	9.0	95.1	78.7	63.6	82.1	96.9	-0.8	5.7	98.6	57.4
4	35.8	-43.1	-52.1	29.1	97.8	97.5	84.8	82.9	-4.7	27.5	58.7	95.1	94.3	97.0	47.5
5	-8.8	-36.8	61.5	91.9	95.6	98.9	76.6	7.8	6.0	48.6	81.0	99.4	95.6	94.9	53.6
6	19.4	-25.9	19.3	88.8	99.9	97.0	89.4	22.0	-3.3	17.5	58.3	99.6	96.8	95.0	49.0
7	19.4	-26.1	19.3	88.8	99.9	97.1	89.5	22.0	-3.2	17.5	58.3	99.6	96.8	95.1	49.0
8	77.1	-4.6	45.6	73.3	97.9	99.1	92.8	68.4	-3.3	14.4	58.6	94.8	98.7	95.9	57.8
9	89.8	-39.6	49.1	56.7	98.7	96.7	95.3	61.7	14.3	13.3	86.7	95.2	97.6	95.6	59.4
10	**90.4**	**49.8**	**48.6**	**22.1**	**97.8**	**96.2**	**94.3**	**50.7**	**25.1**	**27.9**	**41.3**	**83.6**	**91.8**	**90.6**	**59.6**
w_i	0.049	0.07	0.053	0.049	0.049	0.049	0.032	0.091	0.13	0.098	0.091	0.091	0.091	0.059	

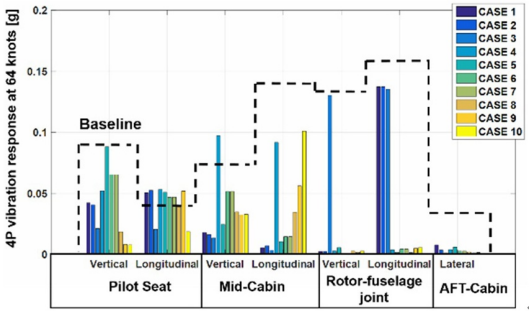

(a) Low-speed flight

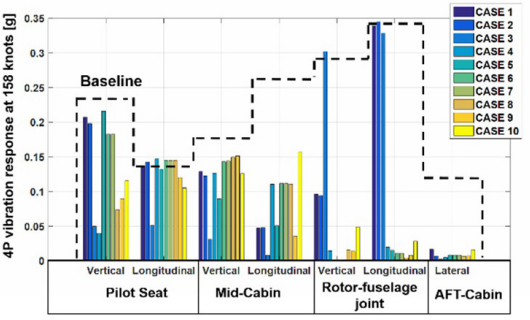

(b) High-speed flight

Fig. 14. Vibration reductions with case study at low- and high-speed flight conditions.

$$J = \sum_{i=1}^{14} (r_i w_i) . \quad (2)$$

Larger weighting factors are assigned to the 4P vibration response reduction rates at high-speed flight condition because the 4P airframe vibration response magnitudes at μ = 0.37 are higher compared to those at μ = 0.15. As summarized in Table 8, the value of J for case 10 is the largest; thus, it is considered the best case (Fig. 15(a)) for reducing the UH-60A airframe vibration responses at both flight conditions.

The 4P airframe vibration reductions using case 10 at low-speed flight condition are 22.05 %-97.83 % (Fig. 15(b)). At the pilot seat, the 4P vibration responses in the vertical and longitudinal directions are reduced by 90.38 % and 49.77 %, respectively, compared to the baseline response without the AVCS. The 4P vertical vibration response is reduced by 48.59 %, and the reduction in the 4P vibration response in the longitudinal direction is 22.05 % at the mid-cabin. At the rotor-fuselage joint, the 4P vibration response in the vertical direction is controlled by 97.83 %, and the 4P vibration response in the longitudinal direction is alleviated by 96.19 %. The reduction in 4P vibration in the lateral direction at the after-cabin is 94.32 %. The vibration responses of the low-speed flight condition are less than 0.1 g at all the locations when AVCS with case 10 is applied. Although case 10 shows moderate vibration reduction performance at low-speed flight condition, the best case at 64 knots (case 6 in Sec. 3.1.2) shows better vibration control performance at most locations. In particular, there is still a relatively high level of 4P longitudinal vibration response at the mid-cabin. However, when applying case 10, the vibration levels are lower than those of the best case for 64 knots at the rotor-fuselage joint (Fig. 15(b)).

The 4P vibration reductions in the high-speed flight condition using case 10 are 25.05 % to 91.81 %, as presented in Fig. 15(c). At the pilot seat, the 4P vibration responses in the vertical and longitudinal directions are reduced by 50.7 % and 25.05 %, respectively. The 4P vibration reductions in the vertical and longitudinal directions are 27.87 % and 41.33 % at the mid-cabin from the baseline response without the AVCS, respectively. At the rotor-fuselage joint, the 4P vibration response reduction in vertical direction is 83.59 % and the 4P vibration response in longitudinal direction is reduced by 91.81 %. The 4P vibration response in the lateral direction the after-cabin is reduced by 90.6 % compared to the baseline response. The 4P vibration responses of the high-speed flight condition at the rotor-fuselage joint and after-cabin are less than 0.1 g, when

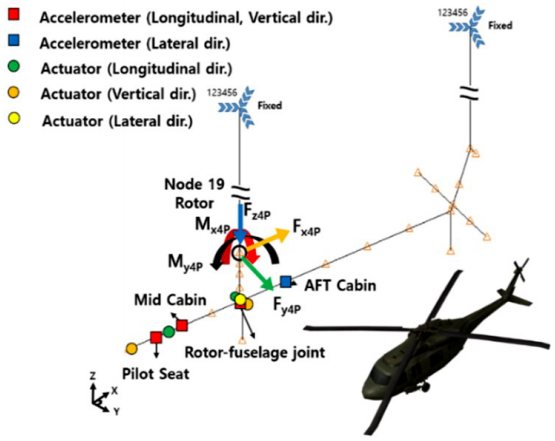

(a) Locations and force directions of CRFGs (case 10)

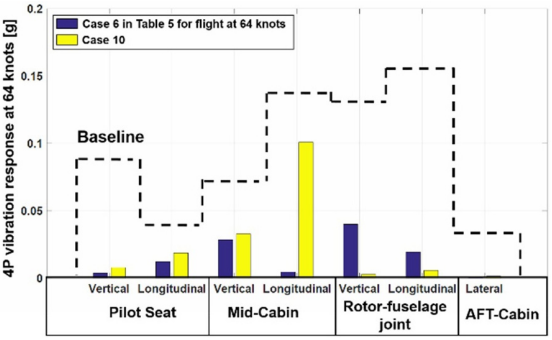

(b) Low-speed flight condition

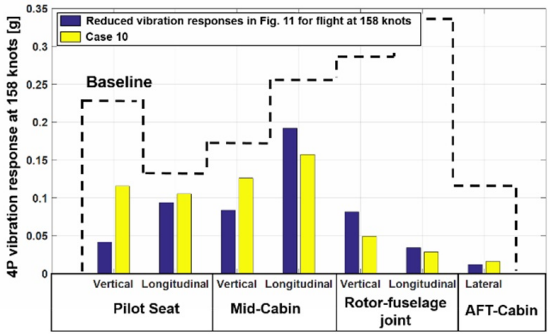

(c) High-speed flight condition

Fig. 15. Reduced 4P vibration responses using AVCS at low- and high-speed flight conditions (case 10).

the AVCS with case 10 is used. The 4P vibration responses at the pilot seat and vertical vibration response at the mid-cabin decrease to approximately to 0.1 g. On the other hand, the 4P vibration response in longitudinal direction at mid-cabin has amplitude of 0.15 g, although the AVCS with case 10 is used. However, this reduction is acceptable because the baseline response in the longitudinal direction at the mid-cabin is greater than 0.26 g. Case 10 can provide lower but similar vibration reduction performances for most accelerometers as compared to the results given in Fig. 11 at 158 knots. As previously discussed, when the AVCS with case 10 is applied to the UH-60A helicopter, the airframe vibration reductions at both low- and high-speed flight conditions are satisfactory.

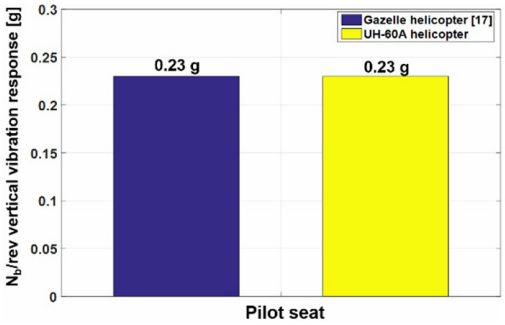

(a) Airframe vibration responses at the pilot seats

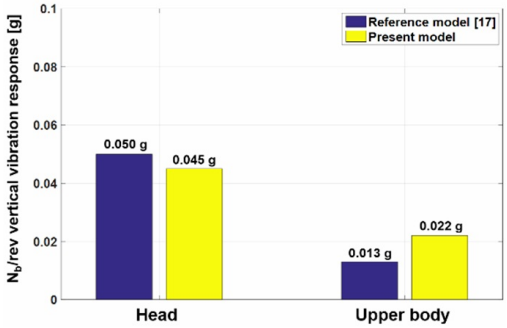

(b) Vibration responses of human body models

Fig. 16. Airframe and human body vibrations at μ = 0.37.

3.2 Vibration reduction of human body

Prior to the investigation of vibration reduction of the human body using AVCS, an analysis technique to predict the vibrations of the human body is validated. Since the N_b/rev airframe vibrations at the pilot seat excite the human body in this work, the human body vibration response magnitudes between two different helicopters may be similar to each other if the airframe vibration response magnitudes are close. The pilot's human body vibrations of the UH-60A helicopter are not available in the public domain; therefore, the vibration responses of the Gazelle helicopter pilot's model [17] are used as a reference model. As shown in Fig. 16(a), the N_b/rev airframe vibrations at the pilot seats are compared for the UH-60A helicopter in this work and Gazelle helicopter [17] at μ = 0.37. As seen in the figure, two N_b/rev airframe vertical vibration response magnitudes at the pilot seat are the same; thus, it is expected that the N_b/rev pilot body vibration responses between two helicopters may be similar. Fig. 16(b) compares the N_b/rev vibration responses of two helicopter pilots' body models. Unlike the present method explained in Fig. 5, the pilot body model in the Ref. [17] was excited only in the vertical direction. In addition, the structural dynamics modeling techniques for the human body to predict human body vibrations are different between two works. Therefore, the N_b/rev vibration responses of two human body models in Fig. 16(b) are not identical although two results in Fig. 16(a) are compared excellently. However, two pilot hu-

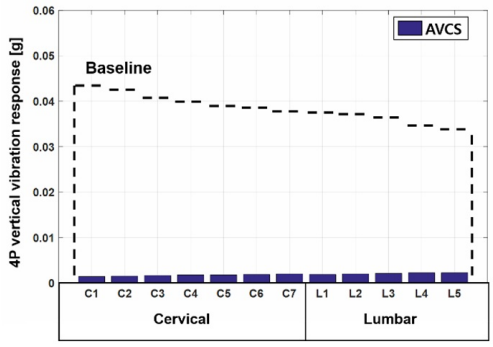

(a) Low-speed flight

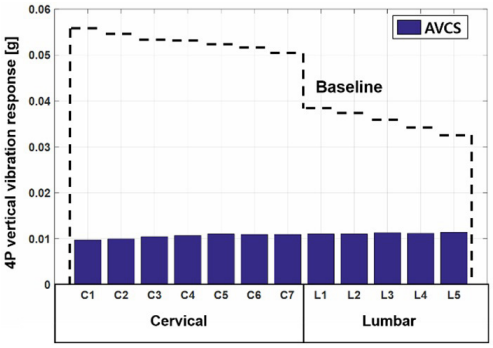

(b) High-speed flight

Fig. 17. Reduced human body model responses using AVCS (case 10).

man body models' vibration responses are comparable. Therefore, the analysis techniques to calculate the helicopter pilot's human body vibration responses in the present study are reasonably well validated.

Fig. 17 shows the vertical vibration reductions at the cervical and lumbar regions of the pilot body when AVCS using case 10, as shown in Fig. 15, is applied to the UH-60A helicopter. Because the cervical spine consists of seven bones (C1-C7) and the lumbar spine is composed of five bones (L1-L5), the average values of the vibration responses of their bones are used to evaluate the present vibration reductions. At a low-speed flight condition, the average vibration reductions at the cervical and lumbar vertebrae are 90.16 % and 89.29 %, respectively, compared to the baseline results (Fig. 17(a)). At high-speed flight condition, when AVCS with case 10 is applied, the average vibration levels of the cervical and lumbar vertebrae are reduced by 72.43 % and 61.23 %, respectively, compared with the baseline response (Fig. 17(b)). Therefore, the AVCS using case 10 alleviates excellently the vertical vibrations of the pilot body and the airframe vibration responses of the UH-60A helicopter at both low- and high-speed flight conditions.

4. Conclusion

In this simulation study, the 4P airframe vibration responses and the pilot body's vertical vibrations of the UH-60A helicopter at low- and high-speed flight conditions (64 and 158 knots) were reduced when AVCS was applied to the airframe. The 4P hub vibratory loads of the UH-60A helicopter were predicted using DYMORE II, which is a flexible multibody dynamics analysis code. The structural dynamics of the helicopter airframe was modeled using 1D elastic beam (CBAR) elements, and its vibration responses were calculated using MSC. NASTRAN. In addition, MSC.NASTRAN was used to model the structural dynamics and predict the vibration responses of the pilot's body. The AVCS used seven accelerometers and five CRFGs. The AVCS framework, using the Fx-LMS algorithm, was constructed using MATLAB Simulink.

A case study was conducted to determine the best locations and vibration cancellation force directions of CRFGs to alleviate the 4P airframe vibration responses at both low- and high-speed flight conditions. As a result, case 10 was considered the best case, which moderately reduced the 4P vibration responses at specified airframe locations (pilot seat, mid-cabin, rotor-fuselage joint, and after-cabin). When AVCS using case 10 was applied to the UH-60A helicopter at low-speed flight condition, the 4P airframe vibration reductions ranged from 22.05 % to 97.83 % and the 4P vibration responses were reduced by 25.05-91.81 % at high-speed flight condition. Furthermore, the pilot body's vertical vibration responses at the cervical and lumbar vertebrae were effectively reduced by applying AVCS. At 64 knots, the vertical vibration responses in the cervical and lumbar regions were reduced by 90.16 % and 89.29 %, respectively, from the baseline response. At 158 knots, the vibration response reductions in the vertical direction at the cervical and lumbar regions were 72.43 % and 61.23 %, respectively. The simulation results indicated that the AVCS using case 10 could moderately control the 4P airframe vibrations of the UH-60A helicopter at both low- and high-speed flight conditions. In addition, it was studied that the AVCS effectively reduced the vertical vibration responses of the pilot body at both flight conditions. Although five CRFGs were used for the UH-60A helicopter airframe, the airframe vibration responses at the specified locations and in the given directions were excellently controlled (or reduced) and a human body's vibrations at the pilot seat, in both low- and high-speed flights. However, it is noteworthy that these vibration reductions do not mean the vibration reductions at all the locations and in all the directions of both the helicopter airframe and human body. However, the present AVCS simulation was performed without considering interactions between the rotor, fuselage, and pilot body, since one-way coupling method was applied in this work. Although these interactions may not significantly effect on vibration responses of the helicopter airframe and human body, more sophisticated analyses considering these interactions will be conducted in the near future. In addition, a 3D finite element fuselage model will be used for active vibration reductions in the helicopter airframe and human body.

Acknowledgments

This study was supported by the Basic Science Research Pro-

gram through the National Research Foundation of Korea (NRF) funded by the Ministry of Education (2020R1I1A3071793). This study was supported by the Basic Science Research Program funded by the Ministry of Science and ICT (2021R1A5A 1031868). Part of this paper was presented at the 2021 Korean Society for Aeronautical and Space Sciences Fall conference, Korea, Samcheok, November 11-19, 2021.

References

[1] D.-H. Kim, T.-J. Kim, S.-U. Jung and D.-I. Kwak, Test and simulation of an active vibration control system for helicopter applications, *International Journal of Aeronautical and Space Sciences,* 17 (3) (2016) 442-453.

[2] R. Blackwell and T. Millott, Dynamics design characteristics of the sikorsky X2 technology™ demonstrator aircraft, *Proc. of The American Helicopter Society 64th Annual Forum*, Quebec, Canada (2008).

[3] T. A. Millott, R. K. Goodman, J. K. Wong, W. A. Welsh, J. R. Correia and C. E. Cassil, Risk reduction flight test of a pre-production active vibration control system for the UH-60M, *Proc. of The American Helicopter Society 59th Annual Forum*, Arizona, USA (2003).

[4] R. K. Goodman and T. A. Millott, Design, development, and flight testing of the active vibration control system for the Sikorsky S-92, *Proc. of The American Helicopter Society 56th Annual Forum*, Virginia, USA (2000).

[5] M. A. Rangacharyulu and M. J. Moore, Flight vibration testing of the V-22 tiltrotor aircraft, *47th American Helicopter Society International Annual Forum*, Arizona, USA (1991).

[6] Y.-L. Lee, D.-Y. Kim, D.-H. Kim, S.-B. Hong and J.-S. Park, Vibration reduction simulations of UH-60A helicopter airframe using active vibration control system, *Journal of The Korean Society Aeronautical and Space Sciences*, 48 (6) (2020) 443-453.

[7] J. Adam, *Results of NVG-induced Neck Strain Questionnaire Study in CH-146 Griffon Aircrew*, Defense Research and Development Canada Toronto, NRDC-TR-2004-153 (2004).

[8] K. Anderen, R. Baardsen, I. Dalen and J. P. Larsen, Long-term effects of exercise programs among helicopter pilots with flying related LBP, *Journal of Back and Musculoskeletal Rehabilitation*, 31 (1) (2018) 1-13.

[9] J.-S. Park, Validation of rotor load analysis using flexible multibody dynamics with multiple wake panels for low-speed flights, *International Journal of Aeronautical and Space Science*, 19 (4) (2018) 863-877.

[10] O. A., Bauchau, *DYMORE II User's Manual*, Georgia Institute of Technology (2006).

[11] W. G. Bousman and R. M. Kufeld, *UH-60A Airloads Catalog*, NASA TM-2005-2312827 (2005).

[12] T. Norman, R. Peterson, P. Shinoda and A. Datta, Full-scale wind tunnel test of the UH-6A airloads rotor, *Proc. of The American Helicopter Society 67th Annual Forum,* Virginia Beach, Virginia, USA (2011).

[13] J.-S. Park, S.-N. Jung and S.-H. Park, Airloads validation study for UH-60A rotor using multibody dynamics modeling, *Proc. of The Korean Society for Aeronautical and Space Sciences Fall Conference*, Gyeongju, Korea (2009).

[14] S.-B. Hong, Y.-L. Lee, Y.-M. Kwon, J.-S. Park, J.-S. Kim and D.-H. Kim, Airframe vibration reduction for an unmanned lift-offset compound helicopter using active vibration control system, *International Journal of Aeronautical and Space Sciences*, 23 (1) (2022) 102-114.

[15] F. Idosor and F. Seible, *Comparison of NASTRAN Analysis with Ground Vibration Results of UH-60A NASA/AEFA Test Configuration*, NASA-CR-184565 (1990).

[16] S. Kitazaki and M. J. Griffin, A modal analysis of whole-body vertical vibration, using a finite element model of the human body, *Journal of Sound and Vibration*, 200 (1) (1997) 83-103.

[17] Z. Khaksar, Numerical modelling of the effects of vibration in helicopters for prediction and analysis of human comfort assessment, *Ph.D. Diss.*, University of New South Wales, Australia (2018).

[18] D.-H. Kim, D.-I. Kwak and Q. Song, Demonstration of active vibration control system on a Korean utility helicopter, *International Journal of Aeronautical and Space Sciences*, 20 (1) (2019) 249-259.

Jae-Sang Park received Ph.D. degree in Mechanical and Aerospace Engineering, from Seoul National University, Seoul, Korea in 2006. From 2006 to 2007, he worked as a post doctor at Flight Vehicle Research Center, Seoul National University. From 2008 to 2013, he worked as a Research Professor at Konkuk University, Seoul, Korea. Dr. Park is currently an Associate Professor, Department of Aerospace engineering, Chungnam National University, Daejeon, Korea. His research interests include aerospace structural analyses and rotorcraft aeromechanics analyses.